nature nanotechnology

Review article

https://doi.org/10.1038/s41565-024-01606-4

Engineering colloidal semiconductor nanocrystals for quantum information processing

Received: 5 September 2022

Accepted: 10 January 2024

Published online: 21 March 2024

Check for updates

Jawaher Almutlaq[1], Yuan Liu[2,3], Wasim J. Mir[4], Randy P. Sabatini[2] ✉, Dirk Englund[1] ✉, Osman M. Bakr[4] ✉ & Edward H. Sargent[2,3,5] ✉

Quantum information processing—which relies on spin defects or single-photon emission—has shown quantum advantage in proof-of-principle experiments including microscopic imaging of electromagnetic fields, strain and temperature in applications ranging from battery research to neuroscience. However, critical gaps remain on the path to wider applications, including a need for improved functionalization, deterministic placement, size homogeneity and greater programmability of multifunctional properties. Colloidal semiconductor nanocrystals can close these gaps in numerous application areas, following years of rapid advances in synthesis and functionalization. In this Review, we specifically focus on three key topics: optical interfaces to long-lived spin states, deterministic placement and delivery for sensing beyond the standard quantum limit, and extensions to multifunctional colloidal quantum circuits.

After decades of intensive theoretical and experimental efforts, the field of quantum information science and engineering is at a critical moment. Research areas within the field have expanded, including quantum information processors[1,2], technologies to connect quantum processors by photons[3] and quantum sensing methods[4]. New possibilities are currently being unlocked in fields spanning defence and biomedical research. A gap remains, however, between proof-of-concept demonstrations and engineering commercially viable systems. To realize the next leap in performance, materials and device scaling challenges must be overcome[5].

In this Review, we describe how leveraging the increasingly coherent and controllable atom-like properties of colloidal quantum dots (CQDs) can open disruptive opportunities in emerging quantum information processing (QIP) applications. In particular, we focus on three key topics that exploit the colloidal nature of CQDs: (1) optical interfaces to long-lived spin states, (2) deterministic placement and delivery for sensing, and (3) an emerging opportunity (from 1 and 2), multifunctional colloidal quantum circuits (MCQCs). We review advances that position CQDs closer to achieving the requisite properties for some initial QIP applications. Furthermore, we discuss design opportunities (such as bottom-up assembly methods and emerging synthesis techniques) for increasing coherence, as well as functionalities to address open technical challenges. Moreover, we envision that a process of iterative co-design of CQDs together with quantum control protocols and algorithms will enable new algorithmic quantum materials such as MCQCs that optimally combine form and function.

Single-photon emission in CQDs

A key component, crucial to the functionality of such technologies is the single-photon emitter, which serves as the quantum light source producing individual photons. Numerous materials have already been made to develop a practical single-photon source including colour centres in diamonds[6,7], neutral atoms[8,9], trapped ions[10], two-dimensional materials[11,12], organic molecules[13,14] and semiconducting quantum

[1]Research Laboratory of Electronics, Massachusetts Institute of Technology, Cambridge, MA, USA. [2]Department of Electrical and Computer Engineering, University of Toronto, Toronto, Ontario, Canada. [3]Department of Electrical and Computer Engineering, Northwestern University, Evanston, IL, USA. [4]KAUST Catalysis Center, Division of Physical Sciences and Engineering (PSE), King Abdullah University of Science and Technology (KAUST), Thuwal, Kingdom of Saudi Arabia. [5]Department of Chemistry, Northwestern University, Evanston, IL, USA. ✉e-mail: randy.sabatini@utoronto.ca; englund@mit.edu; osman.bakr@kaust.edu.sa; ted.sargent@northwestern.edu

https://doi.org/10.1038/s41565-024-01606-4

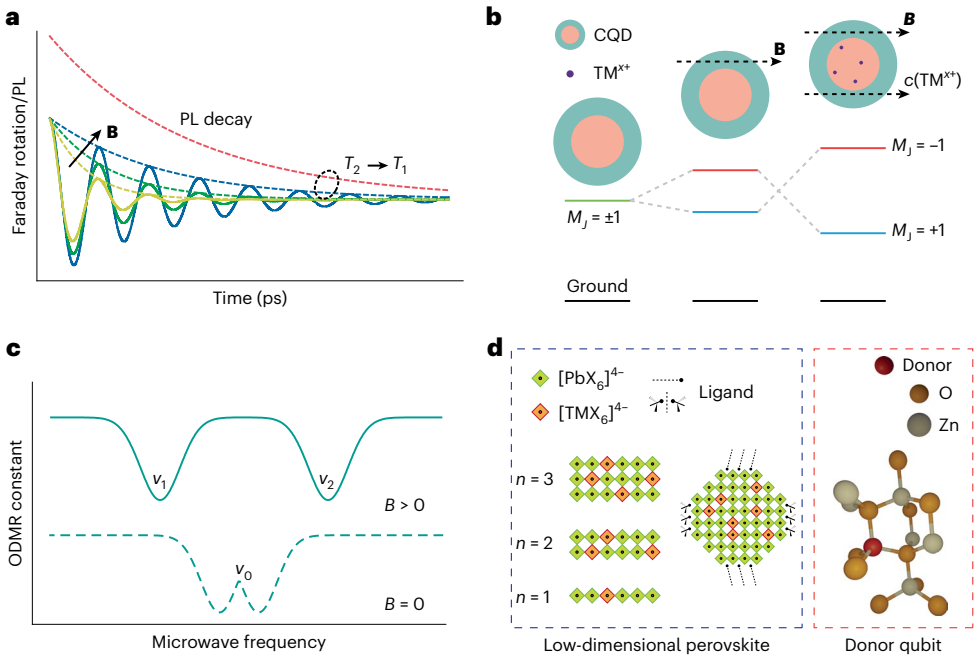

Fig. 1 | Optical interfaces to long-lived spin states. a, Comparison of time-resolved Faraday rotation traces at different magnetic fields (**B**) and photoluminescence (PL) intensity lifetime[101]. **b**, Giant excitonic Zeeman splitting in CQD with and without magnetic doping under a magnetic field. TM, transition metal; M_J, the projection of the total angular momentum along the quantization axis; *c*, the concentration of transition metal dopants in the CQDs. **c**, ODMR spectra measured at zero and non-zero magnetic field where the Zeeman splitting is observed with the corresponding ODMR frequencies 0, v_1 and v_2. **d**, Prospective material platforms that can be used for spin-qubit generation and control. Left: low-dimensional perovskites can be doped with magnetic cations and chiral ligands. *n*, the number of layers in the crystal structure of reduced-dimensional metal halide perovskite materials. Right: donor defects in ZnO crystals.

dots[15,16]. Key performance metrics of single-photon emitters are single-photon purity (that is, antibunching), brightness and indistinguishability[17].

While each class of single-photon emitter has its unique strengths and limitations, semiconductor quantum dots have emerged as a leading solid-state single-photon emitter platform. Solid-state epitaxial quantum dots (EQDs) have demonstrated site-control growth[18], integration of individual EQDs into microcavities[19,20], electrical contacts to make devices and a versatile tunable emission from the visible to the infrared[15]. Although self-assembled EQDs have recently been integrated in photonic circuit platforms for QIP applications[21–23], this hybrid integration comes at the cost of appreciably higher fabrication complexity as well as additional losses (for example, transferring quantum emission from the EQD host semiconductor membrane to the photonic integrated circuit waveguide layer).

These challenges motivate the continued development of CQDs, including perovskite quantum dots (PQDs). CQDs provide simpler and more scalable integration methods into QIP systems. As solution-processed semiconductor nanocrystals, their colloidal nature enables facile synthesis with capabilities of upscaling[24,25]. Through size control and surface engineering, their wavelength response and optical/magnetic properties can be engineered[24]. In addition, while retaining their coherence properties, they can be patterned with well-defined atomic spacing into one-dimensional and two-dimensional arrays and can be integrated easily into a wide range of nanophotonic structures to improve optical control[26–28] including assemblies of quantum emitters[29,30], nanoparticle quantum memories, and auxiliary technologies such as laser amplifiers[31], filters and detectors[32,33].

In terms of single-photon emission, CQDs are aided by fast non-radiative biexciton recombination. These Auger-mediated processes mitigate emission from multiexciton states[34], which would otherwise increase the probability of two-photon emission. Fast multiexciton Auger recombination (for example, 70 ps; ref. 35) thus ensures single-photon purity[36,37], suppressing multi-photon events normalized to an equally bright coherent state by more than 10 times[38]. In 2019, shortly after the report of the bright triplet exciton in lead halide perovskites[39], an optical coherence time (T_2) of 80 ps was demonstrated in $CsPbBr_3$ PQDs[40]. Since then, there has been a growing interest to explore the potential of CQDs as sources of both pure and indistinguishable single photons. Recently, the Hong–Ou–Mandel effect was reported from the interference between indistinguishable single photons of $CsPbBr_3$ PQDs with visibilities of up to 0.56 (ref. 41). Similarly, heavy-metal-free InP-based CQDs have recently been shown to exhibit single-photon purities ($g^{(2)}(0)$) of ~0.08 in the absence of spectral filtering and T_2 = 250 ps (ref. 42). The introduction of a laser cavity, utilizing the Purcell effect, is expected to improve indistinguishability further.

Optical interfaces to long-lived spin states

Some single-photon emitters have associated solid-state electron and nuclear spins, unlocking many opportunities in the field of QIP. A leading example is the nitrogen-vacancy defect in diamond, exhibiting well-defined optical transitions and long-lived spin states[43]. Optically active spin-based solids enable the development of memories as well as localized nanoscale sensing and imaging. Furthermore, the resonantly driven magnetic interaction also enables coherent control of the system's fine and hyperfine states, enabling storage and processing of quantum information akin to methods demonstrated previously in semiconductor quantum dots[44].

Towards this aim, semiconductor nanocrystals containing dopant atoms show great potential. The most common example is a dilute magnetic semiconductor, where a transition metal ion is doped into a semiconductor[45]. Upon the application of a magnetic field, the energy levels associated with spin-up and spin-down states undergo a splitting phenomenon (Zeeman splitting). This leads to a distinct separation in energy levels. Such a configuration forms a two-level system that can serve as a quantum bit (qubit), enabling spin-qubit control

https://doi.org/10.1038/s41565-024-01606-4

BOX 1

Non-classical light emission

Single-photon purity. The probability of a light source to generate no more than one photon per excitation cycle, quantified by the second-order intensity correlation function $g^{(2)}(\tau=0)$ in a Hanbury–Brown–Twiss interferometer[103]. $g^{(2)}(0)$ values close to 0 are often considered a strong indicator of photon antibunching. Currently, the typical $g^{(2)}(0)$ values of CQDs can reach ~0.05 (refs. 40,104).

Determinicity. Deterministic single-photon sources show non-classical behaviour by emitting precisely one photon at a specified time with a high level of certainty[105]. In practice, a single-photon source must have sufficient collection efficiency to be truly deterministic.

Optical coherence time (T_2). The time duration over which the photon maintains its phase[106]. T_2 values up to ~250 ps and 80 ps have been demonstrated for InP-based CQDs and $CsPbBr_3$ PQDs, respectively[40,42].

Purcell effect. The modification of spontaneous emission in an engineered electromagnetic environment[107] (see figure).

Photon indistinguishability. The extent to which two optical pulses are identical in their quantum optical fields. This is represented by observing two identical photons coalesce in the Hong–Ou–Mandel interferometer. Measurements from $CsPbBr_3$ PQDs show a visibility of 0.56 ± 0.12 (ref. 41). In general, photons lose their indistinguishability due to exciton–phonon coupling and interactions with a fluctuating environment over their dephasing time (T_2^*). The overall optical coherence time T_2 is defined as $\frac{1}{T_2} = \frac{1}{2T_1} + \frac{1}{T_2^*}$ (Fig. 1a), where T_1 refers to radiative lifetime[108].

Zeeman splitting. The phenomenon where the energy levels of electrons in semiconductors are split in the presence of a magnetic field due to the interaction between the magnetic field and the spin[109] (Fig. 1b).

Quantum sensor. A system with four necessary attributes: (1) discrete, resolvable energy levels, (2) the possibility to be initialized into a well-known state capable of readout, (3) the ability to be coherently manipulated, and (4) the capability of interactions with a relevant physical quantity[4].

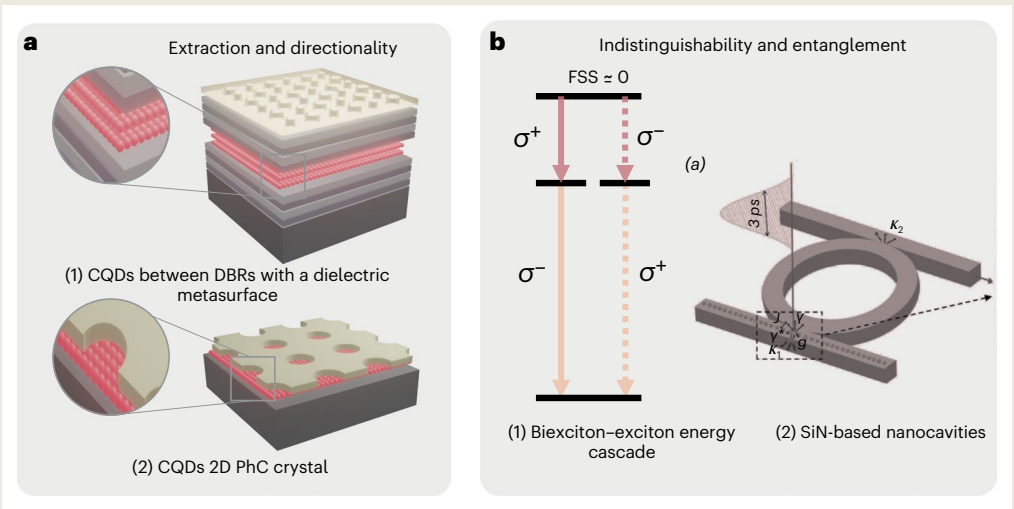

Non-classical light emission. a, Controlled directionality and Purcell enhancement from coupling of CQDs to (1) plasmonic structures and (2) a quasi-two-dimensional cavity. DBR, distributed Bragg reflector; PhC, photonic crystal. **b**, Progress towards indistinguishability and entanglement by (1) post-growth tuning of the biexciton–exciton cascade to reduce the fine-structure splitting and (2) coupling the CQDs to a nanophotonic platform with a nanobeam and ring resonator to improve indistinguishability[110]. FSS, fine structure splitting; σ^+ and σ^-, circularly polarized light; J, the coupling rate between the nanobeam cavity and ring resonator; γ, the decay rate. γ^*, the dephasing rate of the collidal quantum dot; g, the QD to nanobeam cavity coupling rate; κ_1 and κ_2 are the decay rates of the nanobeam cavity and ring resonator, respectively. Panel **b** adapted with permission from ref. 110, American Chemical Society.

and therefore QIP[46–48]. Owing to direct *sp*–*d* exchange between the dopant and semiconductor valence and conduction bands, giant Zeeman splitting occurs (Fig. 1b). Thus, the energy window is expanded (Fig. 1c) between spin states for energy-selective readout based on spin-to-charge conversion[46,49].

Dilute magnetic semiconductor exploration has been carried out extensively with CdSe CQDs and Mn^{2+}, where Zeeman shifts of greater than 50 meV have been shown[50,51]. Single Mn^{2+} magnetic impurities in CdSe have also been explored, providing spin qubits with fewer spin interactions[52]. In contrast, doping in PQDs (as well as quasi-two-dimensional perovskites; Fig. 1d) has not resulted in giant Zeeman splitting[53]. However, instead of a magnetic field, photoexcitation has been used to demonstrate giant Zeeman splitting to the bright triplet state of Mn^{2+}-doped $CsPbBr_3$, providing a potential pathway forwards[54].

Nanoparticles doped instead with rare earth ions (REIs) show photoswitching behaviour that can be promising for QIP[55]. Time-resolved studies have revealed dynamic spin-state transitions where, by tuning the laser excitation from quasicontinuous to pulsed, individual or ensembles of spins can be photoswitched, respectively[56]. Reversible switching of strong light–matter coupling has been also demonstrated for bistable spin-crossover molecular materials[57]. Furthermore, REIs embedded in solid-state hosts and nanocrystals

https://doi.org/10.1038/s41565-024-01606-4

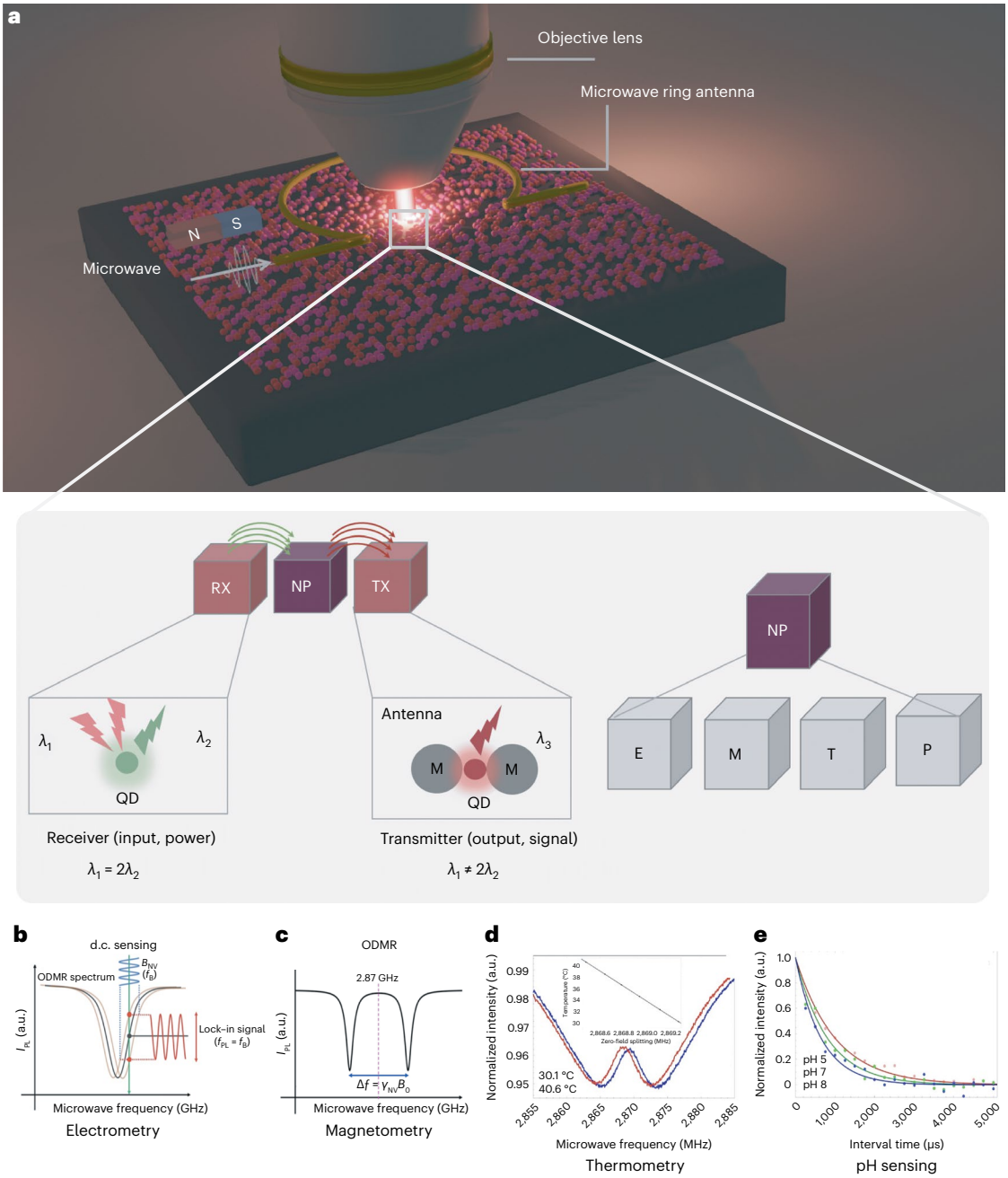

Fig. 2 | Prospects for multicomponent quantum sensing systems. **a**, Top: quantum sensing set-up with a laser beam focused through an objective lens, a microwave ring antenna and a permanent magnet. Bottom: a close-up image of the sensing components showing a receiver (RX), nanoparticle (NP) and transmitter (TX). The upconverted light at the receiver is transferred to the NP where the sensing takes place (or the sensing can be done at the receiver if it has good spin properties). The signal is enhanced at the transmitter before it is received at the detector. **b**–**e**, Based on the characteristics of the NP, different possible sensing modalities include: electrometry (E; **b**), magnetometry (M; **c**), thermometry (T; **d**) and pH sensing (**e**). λ, the excitation/emission wavelength; I_{PL}, photoluminescence intensity; B_{NV}, the magnetic field along the nitrogen-vacancy centre; f_B, the frequency of the magnetic field; f_{PL}, the frequency of photoluminescence; Δf, the shift of the photoluminescence frequency; γ_{NV}, the gyromagnetic ratio of the nitrogen-vacancy centre; B_0, the applied magnetic field strength along a nitrogen-vacancy axis. The inset in Fig. 2e shows how the zero-field splitting value varies with the measured temperature, which is modelled using a linear function. Panels adapted with permission from: **b**,**c**, ref. 102, under a Creative Commons licence CC BY 4.0; **d**,**e**, ref. 78, under a Creative Commons licence CC BY 4.0.

have highly coherent intra-4*f* optical and spin transitions suitable for a wide range of quantum applications, including quantum memories and transduction[58–60]. However, a notable challenge arises from their long lifetimes, which leads to low emission rates[59]. Recent advancements have focused on enhancing the low emission rates of REIs. This enhancement is achieved by integrating the ions with optical cavities and Fabry–Pérot resonators, which effectively shortens the lifetimes (T_1) of the emission while simultaneously increasing the fluorescence yield. This has enabled single-shot readout and spin manipulation of optically addressable single REIs[61–64].

In addition to metal doping, other routes are available to improve QIP applications via the addition of charge donors and acceptors. PQDs have been functionalized with anthraquinone molecules, which act as an electron acceptor[65]. After photoexcitation, anthraquinone extracts an electron from the PQD, which then exhibits a long-lived hole spin precession of hundreds of picoseconds. Neutral shallow

https://doi.org/10.1038/s41565-024-01606-4

BOX 2

Semiconductor nanocrystal basics

Semiconductor quantum dots. Isolated nanometre-sized crystals that show a quantum confinement effect, leading to discrete energy levels and emission of quantized light[111,112] (panel **a**). Depending on their fabrication methods, these can be solid-state EQDs or CQDs.

Colloidal quantum dots (CQDs). Solution-processed semiconductor quantum dots that are stabilized and dispersed in non-polar solvents with the help of long-chain organic ligands[25]. Upon perturbation with bias or light, CQDs show a very bright luminescence on account of exciton confinement, with quantum efficiency that can reach near unity[24].

Types of CQD. CQDs are commonly classified as II–VI (CdS, ZnS and so on) III–V (InP, InAs and so on) or IV–VI (PbS, PbSe and so on) CQDs based on the periodic table groups[112,113]. Another class of CQDs is based on metal halide perovskites ($APbX_3$; A=Cs, CH_3NH_3; X=Cl, Br, I) known as PQDs[113]. Alloyed CQDs constitute a subclass that benefit from composition-dependent bandgap tuning in addition to quantum size effects on bandgap. CQDs can emit in the ultraviolet, visible, near-infrared or mid-infrared region of the electromagnetic spectrum depending on the class and particular type/composition of nanocrystal.

Synthesis of CQDs. The synthesis of CQDs is widely carried out using three popular methods: hot injection, thermal annealing and ligand-assisted re-precipitation (LARP) methods[114]. The hot injection method is very efficient in obtaining monodisperse particles by separating the nucleation and growth phases of CQDs, allowing more control over the size and shape of CQDs. This method works well for II–VI and IV–V CQDs, and PQDs. In the thermal annealing method, annealing at a high temperature promotes simultaneous nucleation and growth of CQDs[115]. This method relies on the use of highly reactive precursors and has been used to synthesize III–V CQDs, which are otherwise challenging to synthesize via the hot injection method. The LARP method works on a principle that involves the precipitation of reactant species from polar to non-polar media with the help of organic ligands[113]. Like the thermal annealing method, the LARP method provides less control over size and shape of particles.

CQDs solids. Assembly of CQDs into solids on a desired substrate can be achieved via well-established techniques such as spin-coating, dip-coating, blade-coating and so on[26,116]. CQDs have a tendency to self-assemble onto a substrate while also adapting ordered structures (for example, upon mixing two different types of material)[26,116] (panel **b**). The 'pick and place' technique has been used as a proof-of-concept demonstration for deterministic placement[117,118]. Another way of assembly is via a template, and in this type of assembly, CQDs can be placed between two metallic contacts[26,27] (panel **c**).

Blinking. CQDs have a long-standing issue of exhibiting photoluminescence intermittency, vividly observed at a single-particle level, and is commonly termed as blinking[119]. This blinking is detrimental for quantum technologies that demand continuous supply of single photons. Poor surface passivation and the presence of surface dangling bonds contribute substantially to photoluminescence blinking[40].

Surface passivation. The surface passivation of CQDs is crucial to enhance photoluminescence quantum efficiency and to avoid blinking problems[40,119]. In conventional approaches, growing a thick shell on CQDs can effectively suppress the blinking and improve the emission yield of CQDs[120]. A potential outlook would be developing an asymmetric shell around faceted CQDs, which was previously used to demonstrate continuous lasing in CdSe CQDs[121]. In addition to the shelling methods, investigations have been conducted on resurfacing with inorganic polar ligands in III–V[122] and II–VI[123] CQDs. This process facilitates the efficient elimination of trap states by passivating surface defects. Growing a shell onto PQDs remains a challenge. In this context, zwitterionic ligands are commonly used to reduce photoluminescence blinking, enhance stability and demonstrate single-photon emission in PQDs[40,124,125]. Recent studies have shown the growth of an ionic matrix, including perovskite[126] and phenethylammonium bromide[127], onto PQDs. The latter exhibits nearly blinking-free characteristics.

Janus nanoparticles. The integration of two or more components with distinct physical or chemical properties into a single particle. Janus particles have been used as biometric logic gates for drug delivery where one side detects the disease and outputs the signal to the other side that releases the drug after an internal processing[128]. They have also been demonstrated for directional heating, sensing and imaging[129]. The main methods of synthesizing Janus particles include masking (protecting one side while modifying the other), self-assembly (block copolymers in solvents) and phase separation (mixing incompatible phases to form one single nanoparticle)[130].

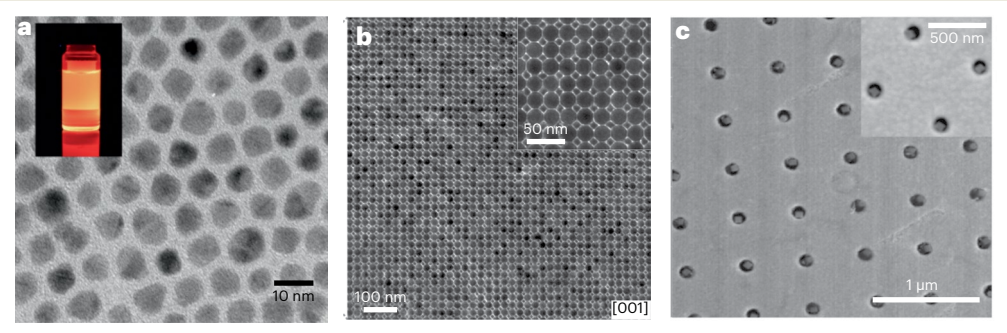

Non-classical light emission and bottom-up assembly and integration. a, Transmission electron microscopy image of monodisperse CdSe/CdS core/shell CQDs with a core (total) size of 3.5 nm (8 nm) and a photoluminescence quantum yield of 80%. Inset: colloidal CdSe/CdS QDs in toluene under UV illumination (ref. 131). **b**, Self-assembly of two different types of CQD adapting a perovskite lattice structure. Inset: a close-up of the superlattice domain[116]. **c**, Template assisted self-assembly of CQDs in between two metallic contacts. Inset: high-resolution scanning electron microscope image of the nanohole arrays[27]. Panels reproduced with permission from: **a**, ref. 131, IEEE, **b**, ref. 116, Springer Nature Ltd. Panel **c** adapted with permission from ref. 27, American Chemical Society.

https://doi.org/10.1038/s41565-024-01606-4

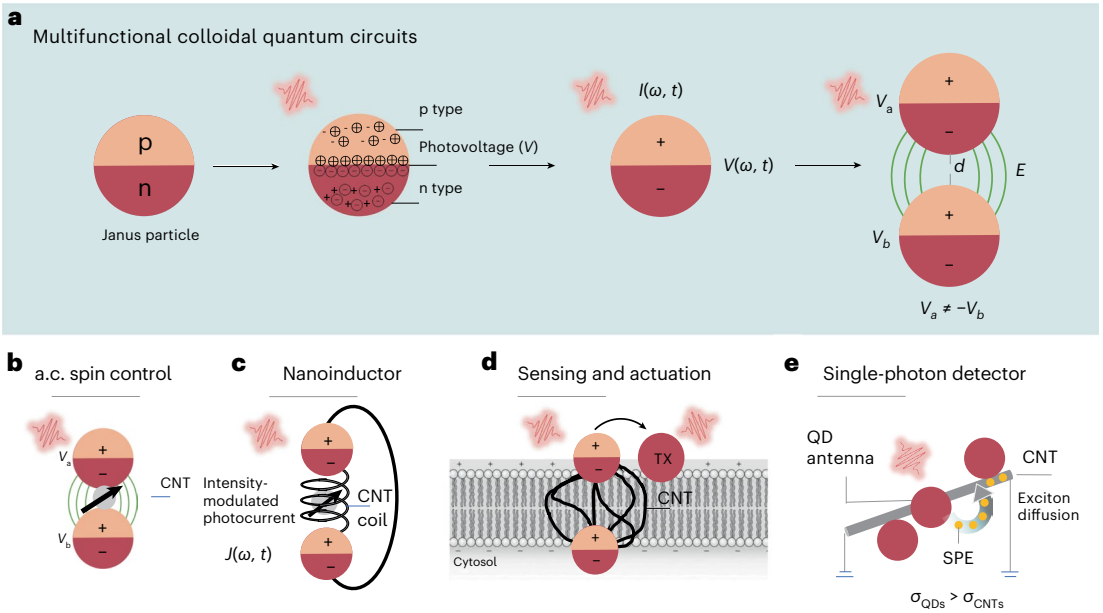

Fig. 3 | Multifunctional colloidal quantum circuits. a, A dual-compartment Janus particle forming a p–n junction. Upon illumination, a photovoltage (V) is created at the interface, which can be modulated through controlling the light intensity $I(\omega, t)$, linking the time and frequency domains. Finally, an electric field is formed at the free space between two Janus particles owing to the opposite doping charges at the sphere ends. The junction forms the building block for **b**–**d**. V_a and V_b, the electrostatic potentials of QD1 and QD2; d, the distance between QD1 and QD2; E, the resulting electric field. **b**, a.c. control of spin states in nanoparticles. **c**, A nanoinductor through the intensity modulated photocurrent $J(\omega, t)$ and coiled carbon nanotubes (CNTs) to control the spin states in nanoparticles. **d**, Simultaneous sensing and actuation in cell membranes. **e**, A single-photon detector where the signal that is received at the QD antenna is transferred to the biased semiconducting carbon nanotubes and the excitons are channelled through exciton diffusion. SPE, single photon emitter; σ_{QDs}, the absorption cross section of QDs; CNTs, carbon nanotubes.

donors, while not yet tested with PQDs or other CQDs, show promise as well. Donor-bound excitons have been formed in silicon, generating qubits with coherence times in minutes, and have more recently been shown in ZnO with a T_1 and T_2 of ~500 ms and 0.05 ms, respectively[66,67]. Depending on the doping density, the application can be tailored from quantum memories to individually selected qubits for quantum computation. We expect that this type of doping will help unlock new opportunities for CQDs.

Deterministic placement and delivery for sensing

Within quantum technology, quantum sensing has emerged as a rapidly advancing application. Unlike conventional sensing methods, which face challenges in further optimizing localization and sensitivity, high-precision quantum sensing highlighted here is based on the utilization of quantum mechanics and spin states to detect the properties of individual particles at the nanoscale (Box 1). Solid-state spin-based sensors have achieved subpicotesla sensitivity[68] and subnanometre resolution in three-dimensional magnetometry[69].

When compared with solid-state quantum sensors, CQDs offer entirely new approaches to address unsolved challenges in sensing. For example, they can serve as receivers in a two-photon absorption set-up with excitation wavelengths in the infrared and upconverted emission in the visible[70] (Fig. 2a). Longer wavelengths are desirable in biosensing as the detection can take place in a deeper area with less damage to the tissue. The upconverted photons can then be used to perform the sensing in the same CQD or transferred to another nanoparticle with good spin properties (in this example, say, a nanodiamond with nitrogen-vacancy centres)[71]. The sensing output signal-to-noise ratio can be further enhanced, if the nitrogen-vacancy centres have low quantum efficiency, by a Förster resonance energy transfer-assisted method to an adjacent CQD-based antenna (for example, CQDs sandwiched between two metal nanoparticles), generating an amplified emission with engineered wavelengths and narrower bandwidth that can be easily read out.

Optically active spin-based nanoparticles allow for different sensing modalities. For example, each of the nanoparticles or spin-doped CQD emitters can individually serve as an optically interfaced electrometer[72] (Fig. 2b). Together, this creates a distributed quantum sensor surface with numerous potential applications, including electric-field noise spectroscopy with optimized spin readout sensitivity and performance beyond the standard quantum limit[73].

Spin-dependent fluorescence can be extended to detect other external stimuli such as temperature and magnetic fields, enabling selectivity to individual sensing quantities[74]. One example is optically detected magnetic resonance (ODMR). In the presence of a magnetic field, the degeneracy of the $|\pm 1\rangle$ state is removed and Zeeman splitting is observed (Fig. 2c). Thermometry is also possible as, in the absence of a magnetic field, the ODMR resonance at the energy of zero-field splitting is temperature-dependent[75–77] (Fig. 2d). Likewise, pH sensing can be obtained via ODMR by observing changes in longitudinal relaxation time (Fig. 2e)[78]. A key requirement, however, is having sufficient spin coherence time (ensemble T_2^* or individual-spin T_2), which can be considered the immunity window of spin coherence against local environmental fluctuations. In general, the sensitivities of these techniques scale with $\frac{1}{\sqrt{T_2^*}}$ (ref. 79). The additional enhancement of sensitivity in CQDs comes from the close proximity of the CQD-based sensor to the surface, compared with other quantum sensing platforms such as solid-state colour centres in diamond and silicon[80]. Nanocrystals can be localized on different target samples through ligand engineering, enabling simultaneous sensing and quantification with subatomic resolution.

Multifunctional colloidal quantum circuits

Beyond the single-particle methods, MCQCs combine the advantages of subcomponents. In MCQCs, the CQDs are arranged in a specific pattern on a substrate and connected by thin metallic wires (for example,

carbon nanotubes to create a circuit)[81]. The circuit can be designed to exhibit specific electronic properties, such as the ability to switch on and off or to amplify electric signals, all with an open geometry and at a scale inaccessible to current lithography tools. We propose using a Janus particle (Box 2) with a dual compartment to form a p–n junction converting the electromagnetic field (that is, laser) into an electric field[82] (Fig. 3a).

Recently, Janus particles with dual Au–TiO_2 compartments have exhibited a light-responsive, self-induced electric field. When illuminated, electron–hole pairs form in the TiO_2 semiconductor hemisphere and separate at the metal–semiconductor boundary. Electrons transfer to the Au metal side, serving as an electron sink, and leave the TiO_2 side positively charged. The resulting photovoltage depends on the potential difference between the compartments (that is, the Schottky barrier height), the light's excitation wavelength and the photon flux[83,84]. Sub-100 nm light-powered Janus nanoparticle motors have also been demonstrated[85]. Critical next steps include investigating how the physical properties scale down to the 10 nm regime.

Another promising component for MCQCs is photoswitching nanoparticles. Recently, photoswitching with high volume of photodarkening–photobrightening cycles and negligible photobleaching has been demonstrated for subångström super-resolution imaging in packed nanoclusters[55]. Such nanoparticles can find applications in conjunction with quantum sensing for dual imaging and enhanced sensing accuracy. Furthermore, they can be used as logic gates in MCQCs analogous to the logic gates in molecular digital information processing[86,87].

Potential MCQCs devices include: localized a.c. field for spin control in qubits (Fig. 3b); nanoinductors (Fig. 3c); simultaneous quantum sensing and actuation to apply action potentials in cell membranes[88] (that is, to trigger a cell to fire) and to provide actuation[89] and feedback (for example, for epilepsy: we could detect an epileptic episode and immediately provide feedback to quench it) (Fig. 3d); and single-photon detectors with CQD antenna and semiconducting carbon nanotubes[90] (Fig. 3e). Finally, while using quantized states in individual quantum sensors can provide high precision and accuracy, and operate with a high spatial resolution inaccessible to classical sensors, sensitivity can be improved past the standard quantum limit, by non-classical, entangled states. The minimum detectable signals can scale as low as $1/N$ for an N-particle quantum state, instead of $1/\sqrt{N}$ for an N-size ensemble measurement. Quantum coherence (from the superposition of multiple energy states) and the more advanced entanglement-enhanced quantum sensing (between indistinguishable and distant quantum systems) would bring the sensitivity closer to the quantum metrology limit (the Heisenberg limit)[91,92]. Creating these entangled states could be done by, perhaps, many-body Rydberg coupling in solids, or by the maximally entangled Greenberger–Horne–Zeilinger states[93,94]. Further opportunities in the field of quantum sensing with CQDs will require continued advances in their synthesis, reproducibility and stability.

Outlook

CQDs have unique challenges as their mesoscopic environment has more fluctuations (that is, is noisier) than in conventional quantum emitter systems that are buried hundreds of nanometres or more within a homogeneous host material. This is currently a major issue for CQDs and leads to decoherence. As the quantum system interacts with the surrounding environment, phonons and other CQDs, the system loses the integrity of quantum information, and the superposed states gradually dephase and collapse into classical states. Additional sources of decoherence include phonon–exciton coupling from high temperature and excitation power[95], as well as exciton–exciton interparticle interactions[42].

Potential solutions include surface passivation to suppress interaction with the environment such as improved isolation of the CQDs through shell and ligand engineering, exploitation of material symmetries to reduce electric-field-induced energy level perturbations (as seen in 'symmetry-protected' group-IV colour centres), and other methods to minimize coupling to phonons and stray electric fields[96]. For coherent spin ground states, magnetically 'quiet' material systems such as ones with spin-neutral isotopic compositions should help.

Another promising direction includes on-chip integration with CQDs. With the rise of photonic integrated circuits for QIP applications[23,97], there is a growing interest in integrating CQDs as single-photon sources. However, unlike epitaxial quantum dots where their integration into photonic structures can be complex and requires high-temperatures, CQDs can be spin-coated onto a passivated silicon substrate for large-area integration with minimal defect density[98] and implemented on complementary metal–oxide–semiconductor circuits enabling scaling and miniaturization[99,100]. Further device integration strategies are already underway.

It is therefore the right time to take advantage of the rapid progress and precise engineering of CQDs to push further the exploration for quantum optics and improve the key metrics of their single-photon emission for QIP applications and devices.

References

1. Chen, W. et al. Scalable and programmable phononic network with trapped ions. *Nat. Phys.* **19**, 877–883 (2023).
2. Zhong, H.-S. et al. Quantum computational advantage using photons. *Science* **370**, 1460–1463 (2020).
3. Kannan, B. et al. On-demand directional microwave photon emission using waveguide quantum electrodynamics. *Nat. Phys.* **19**, 394–400 (2023).
4. Degen, C. L., Reinhard, F. & Cappellaro, P. Quantum sensing. *Rev. Mod. Phys.* **89**, 035002 (2017).
5. Atatüre, M., Englund, D., Vamivakas, N., Lee, S.-Y. & Wrachtrup, J. Material platforms for spin-based photonic quantum technologies. *Nat. Rev. Mater.* **3**, 38–51 (2018).
6. Kurtsiefer, C., Mayer, S., Zarda, P. & Weinfurter, H. Stable solid-state source of single photons. *Phys. Rev. Lett.* **85**, 290–293 (2000).
7. Hausmann, B. J. M. *Nanophotonics in Diamond* (Harvard Univ., 2013).
8. Blinov, B. B., Moehring, D. L., Duan, L.-M. & Monroe, C. Observation of entanglement between a single trapped atom and a single photon. *Nature* **428**, 153–157 (2004).
9. Darquié, B. et al. Controlled single-photon emission from a single trapped two-level atom. *Science* **309**, 454–456 (2005).
10. Stute, A. et al. Tunable ion–photon entanglement in an optical cavity. *Nature* **485**, 482–485 (2012).
11. Gupta, S., Wu, W., Huang, S. & Yakobson, B. I. Single-photon emission from two-dimensional materials, to a brighter future. *J. Phys. Chem. Lett.* **14**, 3274–3284 (2023).
12. Tran, T. T., Bray, K., Ford, M. J., Toth, M. & Aharonovich, I. Quantum emission from hexagonal boron nitride monolayers. *Nat. Nanotechnol.* **11**, 37–41 (2016).
13. Gaither-Ganim, M. B., Newlon, S. A., Anderson, M. G. & Lee, B. Organic molecule single-photon sources. *Oxf. Open Mater. Sci.* **3**, itac017 (2023).
14. Kask, P., Piksarv, P. & Mets, Ü. Fluorescence correlation spectroscopy in the nanosecond time range: photon antibunching in dye fluorescence. *Eur. Biophys. J.* **12**, 163–166 (1985).
15. Arakawa, Y. & Holmes, M. J. Progress in quantum-dot single photon sources for quantum information technologies: a broad spectrum overview. *Appl. Phys. Rev.* **7**, 021309 (2020).
16. Pelton, M. et al. Efficient source of single photons: a single quantum dot in a micropost microcavity. *Phys. Rev. Lett.* **89**, 233602 (2002).
17. Aharonovich, I., Englund, D. & Toth, M. Solid-state single-photon emitters. *Nat. Photon.* **10**, 631–641 (2016).

18. Große, J., von Helversen, M., Koulas-Simos, A., Hermann, M. & Reitzenstein, S. Development of site-controlled quantum dot arrays acting as scalable sources of indistinguishable photons. *APL Photon.* **5**, 096107 (2020).
19. Zadeh, I. E. et al. Deterministic integration of single photon sources in silicon based photonic circuits. *Nano Lett.* **16**, 2289–2294 (2016).
20. Schnauber, P. et al. Indistinguishable photons from deterministically integrated single quantum dots in heterogeneous GaAs/Si_3N_4 quantum photonic circuits. *Nano Lett.* **19**, 7164–7172 (2019).
21. Kim, J.-H., Aghaeimeibodi, S., Carolan, J., Englund, D. & Waks, E. Hybrid integration methods for on-chip quantum photonics. *Optica* **7**, 291–308 (2020).
22. Larocque, H. et al. Tunable quantum emitters on large-scale foundry silicon photonics. Preprint at https://arxiv.org/abs/2306.06460 (2023).
23. Elshaari, A. W., Pernice, W., Srinivasan, K., Benson, O. & Zwiller, V. Hybrid integrated quantum photonic circuits. *Nat. Photon.* **14**, 285–298 (2020).
24. Talapin, D. V., Lee, J.-S., Kovalenko, M. V. & Shevchenko, E. V. Prospects of colloidal nanocrystals for electronic and optoelectronic applications. *Chem. Rev.* **110**, 389–458 (2010).
25. Boles, M. A., Ling, D., Hyeon, T. & Talapin, D. V. The surface science of nanocrystals. *Nat. Mater.* **15**, 141–153 (2016).
26. Kagan, C. R., Bassett, L. C., Murray, C. B. & Thompson, S. M. Colloidal quantum dots as platforms for quantum information science. *Chem. Rev.* **121**, 3186–3233 (2020).
27. Saboktakin, M. et al. Plasmonic enhancement of nanophosphor upconversion luminescence in Au nanohole arrays. *ACS Nano* **7**, 7186–7192 (2013).
28. Uppu, R. et al. Scalable integrated single-photon source. *Sci. Adv.* **6**, eabc8268 (2020).
29. Kang, C. & Honciuc, A. Self-assembly of Janus nanoparticles into transformable suprastructures. *J. Phys. Chem. Lett.* **9**, 1415–1421 (2018).
30. Hao, Q., Lv, H., Ma, H., Tang, X. & Chen, M. Development of self-assembly methods on quantum dots. *Materials* **16**, 1317 (2023).
31. Ahn, N. et al. Optically excited lasing in a cavity-based, high-current-density quantum dot electroluminescent device. *Adv. Mater.* **35**, 2206613 (2023).
32. Bao, J. & Bawendi, M. G. A colloidal quantum dot spectrometer. *Nature* **523**, 67–70 (2015).
33. Livache, C. et al. A colloidal quantum dot infrared photodetector and its use for intraband detection. *Nat. Commun.* **10**, 2125 (2019).
34. Klimov, V. I., Mikhailovsky, A. A., McBranch, D. W., Leatherdale, C. A. & Bawendi, M. G. Quantization of multiparticle Auger rates in semiconductor quantum dots. *Science* **287**, 1011–1014 (2000).
35. Chandrasekaran, V. et al. Nearly blinking-free, high-purity single-photon emission by colloidal InP/ZnSe quantum dots. *Nano Lett.* **17**, 6104–6109 (2017).
36. Michler, P. et al. Quantum correlation among photons from a single quantum dot at room temperature. *Nature* **406**, 968–970 (2000).
37. Hu, F. et al. Superior optical properties of perovskite nanocrystals as single photon emitters. *ACS Nano* **9**, 12410–12416 (2015).
38. Zhu, C. et al. Room-temperature, highly pure single-photon sources from all-inorganic lead halide perovskite quantum dots. *Nano Lett.* **22**, 3751–3760 (2022).
39. Becker, M. A. et al. Bright triplet excitons in caesium lead halide perovskites. *Nature* **553**, 189–193 (2018).
40. Utzat, H. et al. Coherent single-photon emission from colloidal lead halide perovskite quantum dots. *Science* **363**, 1068–1072 (2019).
41. Kaplan, A. E. K. et al. Hong–Ou–Mandel interference in colloidal $CsPbBr_3$ perovskite nanocrystals. *Nat. Photon.* **17**, 775–780 (2023).
42. Proppe, A. H. et al. Highly stable and pure single-photon emission with 250 ps optical coherence times in InP colloidal quantum dots. *Nat. Nanotechnol.* **18**, 993–999 (2023).
43. Balasubramanian, G. et al. Ultralong spin coherence time in isotopically engineered diamond. *Nat. Mater.* **8**, 383–387 (2009).
44. Hanson, R. et al. Zeeman energy and spin relaxation in a one-electron quantum dot. *Phys. Rev. Lett.* **91**, 196802 (2003).
45. Furdyna, J. K. Diluted magnetic semiconductors. *J. Appl. Phys.* **64**, R29–R64 (1988).
46. Elzerman, J. M. et al. Single-shot read-out of an individual electron spin in a quantum dot. *Nature* **430**, 431–435 (2004).
47. Burkard, G., Ladd, T. D., Pan, A., Nichol, J. M. & Petta, J. R. Semiconductor spin qubits. *Rev. Mod. Phys.* **95**, 025003 (2023).
48. Zhang, X. et al. Semiconductor quantum computation. *Natl Sci. Rev.* **6**, 32–54 (2019).
49. Piot, N. et al. A single hole spin with enhanced coherence in natural silicon. *Nat. Nanotechnol.* **17**, 1072–1077 (2022).
50. Beaulac, R., Archer, P. I., Ochsenbein, S. T. & Gamelin, D. R. Mn^{2+}-doped CdSe quantum dots: new inorganic materials for spin-electronics and spin-photonics. *Adv. Funct. Mater.* **18**, 3873–3891 (2008).
51. Archer, P. I., Santangelo, S. A. & Gamelin, D. R. Direct observation of *sp–d* exchange interactions in colloidal Mn^{2+}- and Co^{2+}-doped CdSe quantum dots. *Nano Lett.* **7**, 1037–1043 (2007).
52. Barrows, C. J., Fainblat, R. & Gamelin, D. R. Excitonic Zeeman splittings in colloidal CdSe quantum dots doped with single magnetic impurities. *J. Mater. Chem.* **5**, 5232–5238 (2017).
53. Neumann, T. et al. Manganese doping for enhanced magnetic brightening and circular polarization control of dark excitons in paramagnetic layered hybrid metal-halide perovskites. *Nat. Commun.* **12**, 3489 (2021).
54. Lohmann, S.-H., Cai, T., Morrow, D. J., Chen, O. & Ma, X. Brightening of dark states in $CsPbBr_3$ quantum dots caused by light-induced magnetism. *Small* **17**, 2101527 (2021).
55. Lee, C. et al. Indefinite and bidirectional near-infrared nanocrystal photoswitching. *Nature* **618**, 951–958 (2023).
56. Tran, N. M., Palluel, M., Daro, N., Chastanet, G. & Freysz, E. Time-resolved study of the photoswitching of gold nanorods coated with a spin-crossover compound shell. *J. Phys. Chem. C* **125**, 22611–22621 (2021).
57. Zhang, L. et al. Reversible switching of strong light–matter coupling using spin-crossover molecular materials. *J. Phys. Chem. Lett.* **14**, 6840–6849 (2023).
58. Fernandez-Gonzalvo, X., Chen, Y.-H., Yin, C., Rogge, S. & Longdell, J. J. Coherent frequency up-conversion of microwaves to the optical telecommunications band in an Er:YSO crystal. *Phys. Rev. A* **92**, 062313 (2015).
59. Kolesov, R. et al. Optical detection of a single rare-earth ion in a crystal. *Nat. Commun.* **3**, 1029 (2012).
60. Hedges, M. P., Longdell, J. J., Li, Y. & Sellars, M. J. Efficient quantum memory for light. *Nature* **465**, 1052–1056 (2010).
61. Ulanowski, A., Merkel, B. & Reiserer, A. Spectral multiplexing of telecom emitters with stable transition frequency. *Sci. Adv.* **8**, abo4538 (2022).
62. Kindem, J. M. et al. Control and single-shot readout of an ion embedded in a nanophotonic cavity. *Nature* **580**, 201–204 (2020).
63. Zhong, T. et al. Optically addressing single rare-earth ions in a nanophotonic cavity. *Phys. Rev. Lett.* **121**, 183603 (2018).
64. Dibos, A. M., Raha, M., Phenicie, C. M. & Thompson, J. D. Atomic source of single photons in the telecom band. *Phys. Rev. Lett.* **120**, 243601 (2018).
65. Lin, X., Han, Y., Zhu, J. & Wu, K. Room-temperature coherent optical manipulation of hole spins in solution-grown perovskite quantum dots. *Nat. Nanotechnol.* **18**, 124–130 (2023).

66. Viitaniemi, M. L. K. et al. Coherent spin preparation of indium donor qubits in single ZnO nanowires. *Nano Lett.* **22**, 2134–2139 (2022).
67. Saeedi, K. et al. Room-temperature quantum bit storage exceeding 39 minutes using ionized donors in silicon-28. *Science* **342**, 830–832 (2013).
68. Wolf, T. et al. Subpicotesla diamond magnetometry. *Phys. Rev. X* **5**, 041001 (2015).
69. Grinolds, M. S. et al. Subnanometre resolution in three-dimensional magnetic resonance imaging of individual dark spins. *Nat. Nanotechnol.* **9**, 279–284 (2014).
70. Ishii, A. & Miyasaka, T. Upconverting near-infrared light detection in lead halide perovskite with core–shell lanthanide nanoparticles. *Adv. Photon. Res.* **4**, 2200222 (2023).
71. Gong, J., Steinsultz, N. & Ouyang, M. Nanodiamond-based nanostructures for coupling nitrogen-vacancy centres to metal nanoparticles and semiconductor quantum dots. *Nat. Commun.* **7**, 11820 (2016).
72. Vamivakas, A. N. et al. Nanoscale optical electrometer. *Phys. Rev. Lett.* **107**, 166802 (2011).
73. Solntsev, A. S., Agarwal, G. S. & Kivshar, Y. S. Metasurfaces for quantum photonics. *Nat. Photon.* **15**, 327–336 (2021).
74. Aslam, N. et al. Quantum sensors for biomedical applications. *Nat. Rev. Phys.* **5**, 157–169 (2023).
75. Mok, W.-K., Bharti, K., Kwek, L.-C. & Bayat, A. Optimal probes for global quantum thermometry. *Commun. Phys.* **4**, 62 (2021).
76. Kucsko, G. et al. Nanometre-scale thermometry in a living cell. *Nature* **500**, 54–58 (2013).
77. Toyli, D. M., de las Casas, C. F., Christle, D. J., Dobrovitski, V. V. & Awschalom, D. D. Fluorescence thermometry enhanced by the quantum coherence of single spins in diamond. *Proc. Natl Acad. Sci. USA* **110**, 8417–8421 (2013).
78. Segawa, T. F. & Igarashi, R. Nanoscale quantum sensing with nitrogen-vacancy centers in nanodiamonds—a magnetic resonance perspective. *Prog. Nucl. Magn. Reson. Spectrosc.* **134–135**, 20–38 (2023).
79. Rondin, L. et al. Magnetometry with nitrogen-vacancy defects in diamond. *Rep. Prog. Phys.* **77**, 056503 (2014).
80. Taylor, J. M. et al. High-sensitivity diamond magnetometer with nanoscale resolution. *Nat. Phys.* **4**, 810–816 (2008).
81. Vafaeezadeh, M. & Thiel, W. R. Task-specific Janus materials in heterogeneous catalysis. *Angew. Chem. Int. Ed.* **61**, e202206403 (2022).
82. Zehavi, M., Sofer, D., Miloh, T., Velev, O. D. & Yossifon, G. Optically modulated propulsion of electric-field-powered photoconducting Janus particles. *Phys. Rev. Appl.* **18**, 024060 (2022).
83. Dong, R., Zhang, Q., Gao, W., Pei, A. & Ren, B. Highly efficient light-driven TiO_2–Au Janus micromotors. *ACS Nano* **10**, 839–844 (2016).
84. Jang, B. et al. Multiwavelength light-responsive Au/B–TiO_2 Janus micromotors. *ACS Nano* **11**, 6146–6154 (2017).
85. Xuan, M. et al. Near infrared light-powered Janus mesoporous silica nanoparticle motors. *J. Am. Chem. Soc.* **138**, 6492–6497 (2016).
86. Kink, F., Collado, M. P., Wiedbrauk, S., Mayer, P. & Dube, H. Bistable photoswitching of hemithioindigo with green and red light: entry point to advanced molecular digital information processing. *Chem. Eur. J.* **23**, 6237–6243 (2017).
87. Erbas-Cakmak, S. et al. Molecular logic gates: the past, present and future. *Chem. Soc. Rev.* **47**, 2228–2248 (2018).
88. Ding, H. & Ma, Y. Interactions between Janus particles and membranes. *Nanoscale* **4**, 1116–1122 (2012).
89. Huhnstock, R. et al. Translatory and rotatory motion of exchange-bias capped Janus particles controlled by dynamic magnetic field landscapes. *Sci. Rep.* **11**, 21794 (2021).
90. Claussen, J. C., Franklin, A. D., Ul Haque, A., Porterfield, D. M. & Fisher, T. S. Electrochemical biosensor of nanocube-augmented carbon nanotube networks. *ACS Nano* **3**, 37–44 (2009).
91. Xia, Y. et al. Entanglement-enhanced optomechanical sensing. *Nat. Photon.* **17**, 470–477 (2023).
92. Zhou, H. et al. Quantum metrology with strongly interacting spin systems. *Phys. Rev. X* **10**, 031003 (2020).
93. Greenberger, D. M., Horne, M. A. & Zeilinger, A. Going beyond Bell's theorem. Preprint at https://arxiv.org/abs/0712.0921 (2007).
94. Browaeys, A. & Lahaye, T. Many-body physics with individually controlled Rydberg atoms. *Nat. Phys.* **16**, 132–142 (2020).
95. Cai, R. et al. Zero-field quantum beats and spin decoherence mechanisms in $CsPbBr_3$ perovskite nanocrystals. *Nat. Commun.* **14**, 2472 (2023).
96. Udvarhelyi, P. et al. Spectrally stable defect qubits with no inversion symmetry for robust spin-to-photon interface. *Phys. Rev. Appl.* **11**, 044022 (2019).
97. Pelucchi, E. et al. The potential and global outlook of integrated photonics for quantum technologies. *Nat. Rev. Phys.* **4**, 194–208 (2021).
98. Xu, Q. et al. Heterogeneous integration of colloidal quantum dot inks on silicon enables highly efficient and stable infrared photodetectors. *ACS Photon.* **9**, 2792–2801 (2022).
99. Yun, H. J. et al. Solution-processable integrated CMOS circuits based on colloidal $CuInSe_2$ quantum dots. *Nat. Commun.* **11**, 5280 (2020).
100. Dong, M. et al. High-speed programmable photonic circuits in a cryogenically compatible, visible–near-infrared 200 mm CMOS architecture. *Nat. Photon.* **16**, 59–65 (2022).
101. Crane, M. J. et al. Coherent spin precession and lifetime-limited spin dephasing in $CsPbBr_3$ perovskite nanocrystals. *Nano Lett.* **20**, 8626–8633 (2020).
102. Kuwahata, A. et al. Magnetometer with nitrogen-vacancy center in a bulk diamond for detecting magnetic nanoparticles in biomedical applications. *Sci. Rep.* **10**, 2483 (2020).
103. Bromberg, Y., Lahini, Y., Small, E. & Silberberg, Y. Hanbury Brown and Twiss interferometry with interacting photons. *Nat. Photon.* **4**, 721–726 (2010).
104. Lin, X. et al. Electrically-driven single-photon sources based on colloidal quantum dots with near-optimal antibunching at room temperature. *Nat. Commun.* **8**, 1132 (2017).
105. Lounis, B. & Moerner, W. E. Single photons on demand from a single molecule at room temperature. *Nature* **407**, 491–493 (2000).
106. Buckley, S., Rivoire, K. & Vučković, J. Engineered quantum dot single-photon sources. *Rep. Prog. Phys.* **75**, 126503 (2012).
107. Jacob, Z., Smolyaninov, I. I. & Narimanov, E. E. Broadband Purcell effect: radiative decay engineering with metamaterials. *Appl. Phys. Lett.* **100**, 181105 (2012).
108. Varoutsis, S. et al. Restoration of photon indistinguishability in the emission of a semiconductor quantum dot. *Phys. Rev. B* **72**, 041303 (2005).
109. Bockelmann, U., Heller, W. & Abstreiter, G. Microphotoluminescence studies of single quantum dots. II. Magnetic-field experiments. *Phys. Rev. B* **55**, 4469–4472 (1997).
110. Saxena, A. et al. Improving indistinguishability of single photons from colloidal quantum dots using nanocavities. *ACS Photon.* **6**, 3166–3173 (2019).
111. Gaponenko, S. V. *Optical Properties of Semiconductor Nanocrystals* (Cambridge Univ. Press, 1998); https://doi.org/10.1017/CBO9780511524141
112. Klimov, V. I. *Nanocrystal Quantum Dots* (CRC Press, 2017); https://doi.org/10.1201/9781420079272

113. Shamsi, J., Urban, A. S., Imran, M., Trizio, L. D. & Manna, L. Metal halide perovskite nanocrystals: synthesis, post-synthesis modifications, and their optical properties. *Chem. Rev.* **119**, 3296–3348 (2019).
114. Murray, C. B., Kagan, C. R. & Bawendi, M. G. Synthesis and characterization of monodisperse nanocrystals and close-packed nanocrystal assemblies. *Annu. Rev. Mater. Sci.* **30**, 545–610 (2000).
115. Harris, D. K. & Bawendi, M. G. Improved precursor chemistry for the synthesis of III–V quantum dots. *J. Am. Chem. Soc.* **134**, 20211–20213 (2012).
116. Cherniukh, I. et al. Perovskite-type superlattices from lead halide perovskite nanocubes. *Nature* **593**, 535–542 (2021).
117. Abudayyeh, H. et al. Single photon sources with near unity collection efficiencies by deterministic placement of quantum dots in nanoantennas. *APL Photon.* **6**, 036109 (2021).
118. Ratchford, D., Shafiei, F., Kim, S., Gray, S. K. & Li, X. Manipulating coupling between a single semiconductor quantum dot and single gold nanoparticle. *Nano Lett.* **11**, 1049–1054 (2011).
119. Chen, O. et al. Compact high-quality CdSe–CdS core-shell nanocrystals with narrow emission linewidths and suppressed blinking. *Nat. Mater.* **12**, 445–451 (2013).
120. Efros, A. L. & Nesbitt, D. J. Origin and control of blinking in quantum dots. *Nat. Nanotechnol.* **11**, 661–671 (2016).
121. Fan, F. et al. Continuous-wave lasing in colloidal quantum dot solids enabled by facet-selective epitaxy. *Nature* **544**, 75–79 (2017).
122. Xia, P. et al. Sequential co-passivation in inas colloidal quantum dot solids enables efficient near-infrared photodetectors. *Adv. Mater.* **35**, 2301842 (2023).
123. Xiao, P. et al. Surface passivation of intensely luminescent all-inorganic nanocrystals and their direct optical patterning. *Nat. Commun.* **14**, 49 (2023).
124. Krieg, F. et al. Colloidal $CsPbX_3$ (X = Cl, Br, I) nanocrystals 2.0: zwitterionic capping ligands for improved durability and stability. *ACS Energy Lett.* **3**, 641–646 (2018).
125. Mir, W. J. et al. Lecithin capping ligands enable ultrastable perovskite-phase $CsPbI_3$ quantum dots for Rec. 2020 bright-red light-emitting diodes. *J. Am. Chem. Soc.* **144**, 13302–13310 (2022).
126. Liu, Y. et al. Bright and stable light-emitting diodes based on perovskite quantum dots in perovskite matrix. *J. Am. Chem. Soc.* **143**, 15606–15615 (2021).
127. Mi, C. et al. Biexciton-like Auger blinking in strongly confined $CsPbBr_3$ perovskite quantum dots. *J. Phys. Chem. Lett.* **14**, 5466–5474 (2023).
128. Zhao, T. et al. Emulsion-oriented assembly for Janus double-spherical mesoporous nanoparticles as biological logic gates. *Nat. Chem.* **15**, 832–840 (2023).
129. Yi, Y., Sanchez, L., Gao, Y. & Yu, Y. Janus particles for biological imaging and sensing. *Analyst* **141**, 3526–3539 (2016).
130. Safaie, N. & Ferrier, R. C. Jr. Janus nanoparticle synthesis: overview, recent developments, and applications. *J. Appl. Phys.* **127**, 170902 (2020).
131. Xie, W. et al. Colloidal quantum dots enabling coherent light sources for integrated silicon-nitride photonics. *IEEE J. Sel. Top. Quantum Electron.* **23**, 1–13 (2017).

Competing interests

The authors declare no competing interests.

Additional information

Correspondence and requests for materials should be addressed to Randy P. Sabatini, Dirk Englund, Osman M. Bakr or Edward H. Sargent.

Peer review information *Nature Nanotechnology* thanks the anonymous reviewers for their contribution to the peer review of this work.